Journal of Power Sources 246 (2014) 110–116

Contents lists available at ScienceDirect

Journal of Power Sources

journal homepage: www.elsevier.com/locate/jpowsour

Detecting proton exchange membrane fuel cell hydrogen leak using electrochemical impedance spectroscopy method

Ghassan Mousa [a], Farid Golnaraghi [a,*], Jake DeVaal [b], Alan Young [b]

[a] School of Engineering Science, Simon Fraser University, Surrey, BC, Canada V3T 0A3
[b] Ballard Power Systems, 9000 Glenlyon Parkway, Burnaby, BC, Canada V5J 5J9

HIGHLIGHTS

- EIS is able to detect the hydrogen leak through an MEA.
- Impedance signature increases with the increasing rates of leaks.
- The mass transport region increased due to the recombination of oxygen at the cathode.
- EIS cannot detect the leak if it is low or located at the downstream of the MEA.

ARTICLE INFO

Article history:
Received 29 December 2012
Received in revised form
6 June 2013
Accepted 4 July 2013
Available online 24 July 2013

Keywords:
PEM fuel cell
EIS
Hydrogen leak
Oxygen concentration
Differential pressure

ABSTRACT

When a proton exchange membrane (PEM) fuel cell runs short of hydrogen, it suffers from a reverse potential fault that, when driven by neighboring cells, can lead to anode catalyst degradation and holes in the membrane due to local heat generation. As a result, hydrogen leaks through the electrically-shorted membrane-electrode assembly (MEA) without being reacted, and a reduction in fuel cell voltage is noticed. Such voltage reduction can be detected by using electrochemical impedance spectroscopy (EIS). To fully understand the reverse potential fault, the effect of hydrogen crossover leakage in a commercial MEA is measured by EIS at different differential pressures between the anode and cathode. Then the signatures of these leaky cells were compared with the signatures of a no-leaky cells at different oxygen concentrations with the same current densities. The eventual intent of this early stage work is to develop an on-board diagnostics system that can be used to detect and possibly prevent cell reversal failures, and to permit understanding the status of crossover or transfer leaks versus time in operation.

1. Introduction

Fuel cells transform chemical energy into electrical and thermal energy by electrochemical reaction that takes place in between electrodes and an electrolyte. In proton exchange membrane (PEM) fuel cells, hydrogen oxidation takes place on the anode side while oxygen reduction occurs at the cathode. After oxidation, hydrogen protons move from the anode to the cathode with the help of a thin layer of ion-conducting catalyst and electrons flow out of the cell to produce energy. In order to come up with enough power to satisfy the load, fuel cells are usually stacked in series.

Ballard Power Systems uses 6th generation FCvelocity™-HD6 Modules that utilize state of the art automotive Proton Exchange Membrane (PEM) stacks to power many buses around the world. Fuel cell system design targets optimum operating conditions and efficient systems to insure sufficient humidification, and air and fuel supplies. However, if the reactant feed does not respond to the current demand quickly enough, such as during sudden load increases and/or start-up/shutdowns, full or transient fuel starvation may occur causing cathode or anode degradation. Cells containing transfer or crossover leaks are at greater risk of fuel starvation.

Full fuel starvation can result in reverse potential faults, where normal operating cells push current through the fuel starved cell. This causes a rise in the anode potential to the potential required to oxidize water and the anode catalyst carbon support (Equations (1) and (2)). The protons then pass through the membrane to the cathode to produce hydrogen (equation (3)).

$$2H_2O \rightarrow O_2 + 4H^+ + 4e^- \quad (1)$$

$$C + H_2O \rightarrow CO_2 + 2H^+ + 4e^- \quad (2)$$

$$2H^+ + 2e^- \rightarrow H_2. \quad (3)$$

* Corresponding author.
E-mail address: mfgolnar@sfu.ca (F. Golnaraghi).

0378-7753/$ – see front matter © 2013 Published by Elsevier B.V.
http://dx.doi.org/10.1016/j.jpowsour.2013.07.018

During shut-down periods hydrogen is consumed by air that diffuses to the anode catalyst layer. Upon start-up, hydrogen mixes with the stagnant air and creates transient starvation of cells as the hydrogen supply is replenished at the anode. This causes a spike in both the cathode and anode potentials, resulting in oxidation of water and the cathode catalyst carbon support, as described by Equation (2). Tang et al. [1] studied the effect of fuel starvation on the fuel cell during start up and noticed a reduction of the catalysts surface areas.

Carbon oxidation of the catalyst support reduces the catalyst active area due to agglomeration and reduces the catalyst layer thickness, which often causes mass transport degradation. N. Yousfi-Steiner et al. [2] reviewed the causes and consequences of fuel cell starvation faults in detail.

During the reverse potential fault, the safe threshold of hydrogen leaks through the fuel cells can be detected using hydrogen sensors in the downstream cathode exhaust. Unfortunately, those sensors are expensive and not reliable over long periods of time. Thus, a more reliable diagnostic technique is required to monitor hydrogen leakage through fuel cells. Wu et al. [3] reviewed several diagnostic techniques that can be used to detect fuel cells faults. The Cell Voltage Monitoring (CVM) technique measures the voltage of each cell in the stack. However, it cannot be used to detect the voltage on board due to reliability issues. Electrochemical impedance spectroscopy (EIS) is an experimental technique that can be used to perform impedance measurements over a wide frequency range for DC power generation devices. The main advantage of EIS is the possibility to resolve, in the frequency domain, the individual contributions that affect the overall PEM fuel cell performance under load conditions [4].

The authors of this paper are not aware of any EIS study that has been conducted to show the effect of hydrogen leaks through PEM fuel cell. In this study the effect of hydrogen leaks on a single cell were evaluated using an EIS method. In order to increase our understanding of the impedance behavior at different hydrogen leak rates, we compare it with the impedance signatures of reduced oxygen concentrations in the cathode. These faulted impedance signatures will be used in the future to detect reverse potential faults in a stack or the outcomes thereof.

2. Process modeling

2.1. An overview of EIS

EIS usually employs a frequency response analyzer (FRA) to apply either a small AC voltage or current perturbation signal to a cell, and measures its output signal for a wide frequency range. The impedance is calculated by dividing the voltage by current, in the form of a magnitude and phase angle, at each specific frequency.

Impedance spectroscopy has the ability to characterize many of the electrical properties of materials and their interfaces with electrodes. This ability has made the EIS technique widely used in modeling and diagnostics of PEM fuel cells, where individual contributions affecting cell performance can be distinguished by fitting the impedance spectrum into parameters of an equivalent circuit model. Electrical circuits with different configurations, components, and degree of complexity have been proposed in the literature.

The basic equivalent circuit often used to represent fuel cell operation is the Randles circuit shown in Fig. 1, where C_{dl} is the double layer capacitance of the catalyst surface, R_{HF} describes the movement within a conducting media and illustrates the sum of contribution from contact resistance between components and high frequency resistance of the cell components, and R_{ct} is the resistance that occurs when electrons transfer at the electrode/electrolyte interface. R_{ct} decreases when overpotential increases due to the faster oxygen reaction rate. Kang et al. [5] noticed an increase in R_{ct} with increasing the degree of the reverse potential fault in a fuel cell caused by fuel starvation.

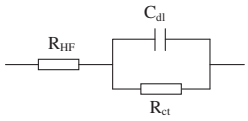

Fig. 1. Randles model.

Nyquist plots show the resistance versus reactance at multiple frequencies, as obtained by the EIS measurements, Fig. 2. The high frequency region of the impedance spectrum represents the high frequency resistance whereas the low frequency region represents the high frequency resistance and charge transfer resistance respectively [6]. At high frequency, the C_{dl} is short circuited and the R_{HF} is measured. As frequency decreases, the impedance becomes a combination of resistance and reactance from the capacitive element. At low frequency, C_{dl} acts like a blocking diode and the total resistance is equal to R_{HF} and R_{ct}.

2.2. Electrical circuit model

More complicated circuits than the Randles circuit are proposed in the literature for different purposes. Others [4,7,8] have added additional to the Randles circuit to include mass transfer effects series connections represent subsequent events while parallel connections represent simultaneous events.

Makharia et al. [9] used a transmission line circuit to include the catalyst layer resistance. Cano-Castillo et al. [10] compared the transmission line circuit with a circuit similar to the ones used by Refs. [4,7], where they added a resistive and capacitive element to the Randles circuit. Both the transmission line and the modified Randles circuit gave reasonable fit with the experimental data.

Andreasen et al. [11] used two circuits, the modified Randles circuit described above, and the other with a constant phase element (CPE) instead of a capacitor in the second circuit. The authors showed that using the circuit with the CPE fitted better to their impedance data. Others [12–14] also replaced capacitive elements with CEPs to adapt their models with the deformed impedance arc. This deformation results from the porous structure of the electrodes where the electron charges are not distributed evenly inside the electrode.

Another equivalent circuit variant [15] represented the mass transport phenomena with a Warburg impedance element in series with the Randles circuit.

In this study it was sufficient to represent the impedance spectra with the modified Randles equivalent circuit shown in Fig. 3, utilizing resistive and capacitive elements to describe both kinetic and mass transport phenomenon. More specifically, R_{mt} describes the oxygen diffusion resistance, while C has been used to describe the

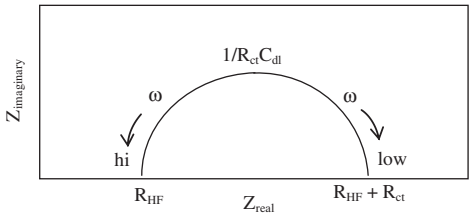

Fig. 2. Nyquist plot of a fuel cell.

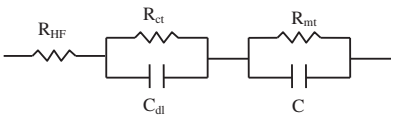

Fig. 3. Equivalent FC circuit for experimental fitting.

diffusion layer in the Pt/C agglomerate structure where oxygen is consumed at the Pt surface [8]. Those parameters represent the cathode side of the cell where oxygen reduction rate (ORR) at the cathode is several orders of magnitude slower than the hydrogen oxidation rate (HOR) [16].

The proposed equivalent circuit yields to the following equation of motion:

$$Z = R_{\mathrm{HF}} + \frac{1}{C_{\mathrm{dl}}(j\omega) + \frac{1}{R_{\mathrm{ch}}}} + \frac{1}{C(j\omega) + 1/R_{\mathrm{mt}}} \tag{4}$$

3. Experimental details

The full-size FCvelocity™-1100 fuel cells were tested at Ballard Power Systems at 20 and 50 A loads. Cells with small, medium and large hydrogen leaks were tested with a differential pressure (dP) of 2, 4, 6 and 8 psig (13.8, 27.6, 41.4 and 55.2 kPa) using air as oxidant. The normal and leaky cells were also tested with different oxygen concentrations; see Table 1 for the test plan details.

To separate the single contributions of the performance loss of the fuel cell during load, impedance measurements were conducted while changing only one variable at a time. All EIS test were made at low currents; 20 A and 50 A to insure that hydrogen leak was not hindered by the increasing content of water resulted from higher ORR at higher loads. Running at low loads insures an adequate hydration on the anode and cathode where water diffuses between those two compartments. This insured that cathodic overpotential was the main contribution to the impedance signature. At higher current densities, anode tends to dry-out as a result of higher protons migrate to cathode carrying water molecules.

Table 1
The test plan.

	Oxygen concentration					
	21 %	18.6 %	16.8 %	14.7 %	12.6 %	10.5 %
Load	Normal dP					Normal cell
	125 A					
	50 A					
	20 A, 0 dP					In and out hydrogen leak
	50 A					Low leak / Med leak / Large leak
	20 A, (2 - 8) dP					
	50 A					
	20 A					

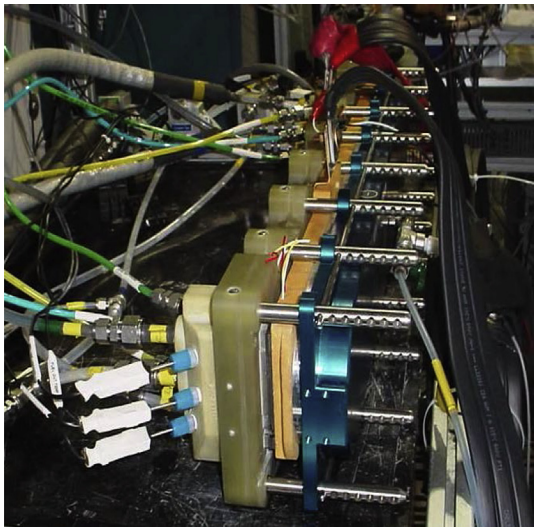

Fig. 4. The single-cell fuel cell stack.

This adds anodic overpotential contribution to the impedance spectra.

To allow a fair comparison between the impedance of leaky cells and the normal cell, hydrogen leakage across the leaky cells was minimized by keeping 0 dP across the holes. All measurements were conducted using Kikusui EIS equipment in galvanostatic mode with a 10% AC amplitude over the frequency range 20 k–80 mHz. EIS measurements were conducted once the stack reached equilibrium for each operating condition tested. In order to avoid the change in current and voltage relationship during measurements, the total frequency sweep of the impedance measurement were conducted in shortest time possible, about 6 min. Thus the system can be assumed to be at steady-state condition during the measurement. To avoid frequency interference, the power supply and loadbank (see Fig. 5) were turned off while measuring the impedance.

Prior to testing, leak rates were evaluated at 0.5 bar (50 kPa) air pressure across the MEA. The MEA was then placed in an open-faced fixture with 3–5 psi dP (20.7–34.5 kPa) dP to identify the holes' location. Submerged in DI water, bubbles appear at the surface of the MEA revealing the location of the leaks.

In testing, temperatures of the anode and cathode were kept equivalent by providing similar coolant flows through the stack. The cell voltage was recorded between the terminals of the stack, which is shown in Fig. 4.

The test bed used a TDI – Dynaload loadbank RBL488 400-600-4000 and Xantrex DC power supply XPR 10-600 connected in series to satisfy the voltage limitation of the loadbank. The Kikusui EIS equipment consisted of an FC impedance meter KFM2150 and three electronic loads PLZ664WA. The loadbank and power supply were

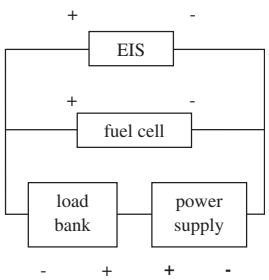

Fig. 5. Schematic view of the test bed.

connected to the fuel cell and EIS machines in parallel, as shown in Fig. 5. This configuration provided the required load by using either the EIS equipment or the test station loadbank between test periods. The power supply was used to overcome voltage limitations of the loadbank when higher voltage was needed for higher current testing.

The test bed controlled and monitored the stack temperature, fuel and air humidity, gas flow rates, pressures, and load current. Two MFC's for oxidant and fuel were installed in the test bed to allow low and high flow rates. Gas mixers were used in this experiment to control the oxygen and hydrogen concentrations balanced with nitrogen. The use of mixers allowed the testing of various oxygen and hydrogen concentrations while maintaining constant flow rates, Table 2. Using constant flows made the EIS measurements more stable due to improved water management.

4. Results and discussion

Four cells in total were used in this study; a normal working cell and three leaky cells. The leaky cells were selected from working bus modules with low, medium and high crossover leak rates of approximately 50, 300 and 500 cm^3 min^{-1}, with air at 0.5 barg. All leak locations were determined to be at the inlet side of the fuel cells. Outlet port leak tests were conducted by switching the inlet and outlet ports of the stack. To approximate the operating conditions of the stack, 1 standard L min^{-1} (slpm) fuel flow at a 66% hydrogen concentration was used with a 20 A load.

4.1. Changing load

Similar to the studies done by Refs. [11,12,17], we noticed a reduction in impedance with the increasing amounts of loads, see Fig. 6. However, the mass transport part of the impedance increased with the increasing of the load. This increase in the mass transfer at high currents is usually associated with improper water management due to higher ORR or insufficient reactant feeding. This increase can be explained by the logarithmic kinetic response to current commonly described by Tafel kinetics:

$$E = a \log\left(i/i_o\right) \tag{5}$$

where

E: electrode potential (V)
i: current density (A)
i_o: exchange current density (A)
a: Tafel constant

4.2. Changing oxygen concentration

Lebeak Jespersen et al. [14] studied the effect of air and hydrogen stoichiometry on the impedance. With the lower air stoichiometry impedance signatures increases. This increase was

Table 2
The fuel cell operating conditions.

Loads (A)		125	50	20
Hydrogen parameters	Fuel flow (SLPM)	2.43	1.42	0.66
	Fuel In Press (kPa)	94	68	57
	Fuel Dew Point (°C)	62.07	62.74	61.74
Oxygen parameters	Ox flow (SLPM)	3.89	1.78	1.03
	Air In Pressure (kPa)	80	55	43
	Air Dew Point (°C)	60.83	61.29	60.2

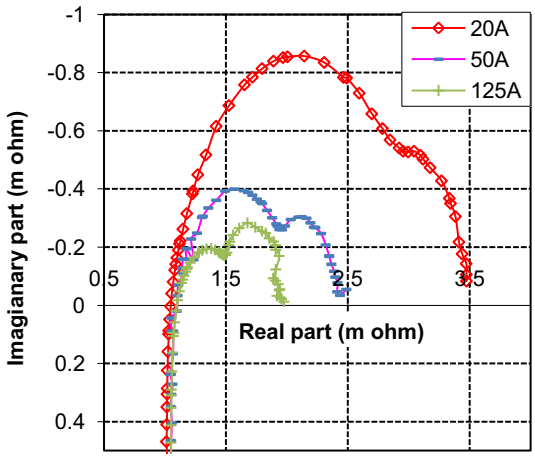

Fig. 6. Impedance of a normal cell at 20, 50 and 125 A load.

mainly noticed at the mass transport part. With the lower hydrogen stoichiometry the authors noticed no change in the impedance signatures. They concluded that changing air stoich has a dramatic effect on the ORR while changing hydrogen stoich has limited effect on the HOR and thus on the overall performance of the fuel cell.

Boillot et al. [18] studied similar effects on the impedance by diluting hydrogen and oxygen respectively with nitrogen to change the fuel and oxidant concentrations. In case of hydrogen dilution, the authors noticed an increase of the impedance arc at high and medium frequency regions with higher amounts of dilution. However, the difference in impedance with lower hydrogen concentration was very small. In case of oxygen dilution, the authors noticed a reduction in impedance with higher amount of oxygen concentrations, more than 21%, at the low frequency region. However, the effect of concentration lower than the amount of oxygen in air was not considered. In our study, we reduced the amount of oxygen concentration until the stack reached starvation.

Similar to those two studies, the effect of hydrogen dilution in our impedance signatures were minimal and major changes in the impedance with different hydrogen concentrations were not apparent. With lower amounts of oxygen concentrations, we found a steady increase in the impedance. This increase was mostly at the mass transport region, second arc. When oxygen concentration was reduced to an amount less than needed by the stack, air starvation occurred and the impedance increased significantly, as shown in Fig. 7. At concentrations lower than 10% oxygen, the cell voltage was unstable and impedance could not be measured.

Because the leaky cells used in the experiment were rejected from operating bus modules, their impedances were bigger than the impedance of the normal cell due to degradation, see Fig. 8. For the sake of comparison, the impedance spectra were normalized by the high frequency resistance of 1.34 +/− 0.25 m ohm.

4.3. Changing delta pressure

Khorasani et al. [19] and Tian et al. [20] studied the output voltage and pressure difference between anode and cathode to localize the leaky MEA in a small stack. The authors noticed a decrease in the voltage of the defected cell when increasing the anode pressure. This decrease in voltage resulted from the increased amount of hydrogen leak rate through the MEA which results in depletion of oxygen in the cathode.

In our study, leak rates were controlled by adjusting dP across the hole. The higher the dP, the greater the amount of hydrogen leaking through the MEA. When leaks occurred, the charge transfer

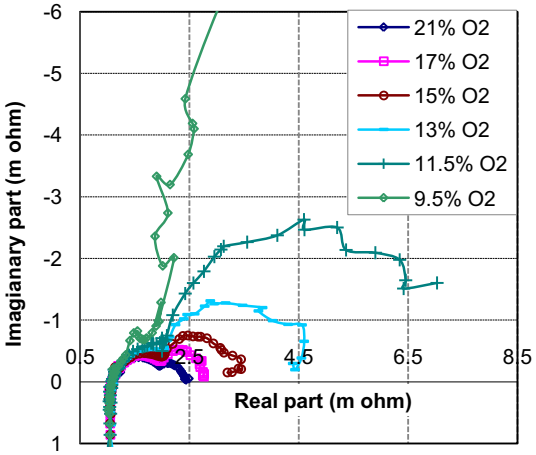

Fig. 7. Impedance of a normal cell at 50 A load.

impedance, first arc decreased and its second arc increased, see Figs. 9 and 10. The reduction of the charge transfer is similar to the reduction of impedance at high load currents, and the increase of impedance second arc is similar to the increase of impedance at low oxygen concentrations. This similarity in impedance drives us to the conclusion that, at high dP, there is a greater internal parasitic current due to greater hydrogen crossover that affects the kinetics. The greater current generated by the catalyst (loadbank and parasitic) drives the charge transfer arc down due to the logarithmic Tafel relationship between voltage and current described earlier. Further when hydrogen leakage increases and reacts at the cathode, oxygen mass transport limitation increases as shown by the mass transport curve.

4.4. Changing hole location

Increasing leak rates at 50 A increased R_{mt} but did not affect R_{ct} where the parasitic current is a smaller portion of the total current, see Fig. 11. As expected, no change in the parameters were noticed with the increasing leak rates at the outlet port, except at high hydrogen leak, where most of fuel recombined with air throughout the stack length. In all cases C_{dl} changed in a small range. This reflects the intact property of the MEA material throughout the tests.

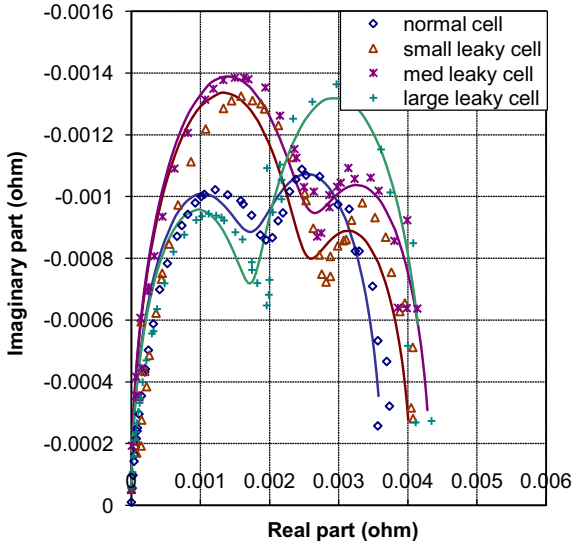

Fig. 8. 20 A impedance of the normal cell and leaky cells with inlet holes for 13% O2 concentration.

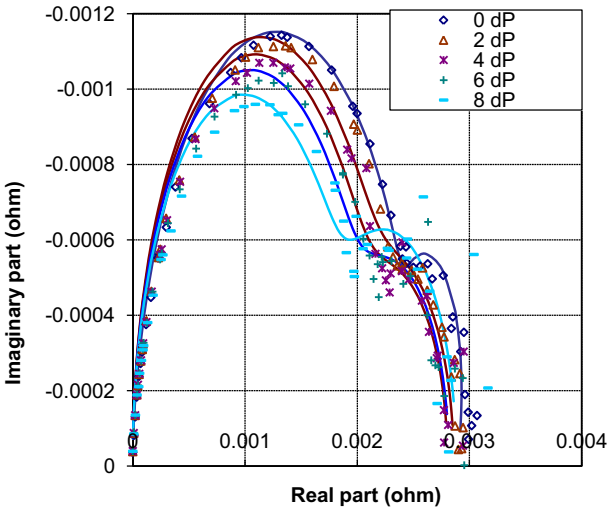

Fig. 9. 20 A impedance of the medium leaky with holes located at the inlet at different dP.

The signatures of leak rates at the outlet of the stack were barely changed at 20 A. Thus their associated parameters were omitted.

The effect of hole location on the impedance agrees with our other studies – outside the scope of this work – that examined the recombination effectiveness of hydrogen transfer leaks in the upstream and downstream of the cathode on the performance of a stack. It was noticed that increasing the hydrogen concentration at the cathode inlet reduced the voltage of a cell gradually up to a limit where cell voltage became unstable and hydrogen appeared at the oxidant outlet. When the hole was placed at the cell air outlet, the cell didn't suffer much air starvation and most of the hydrogen leaked through the hole was measured at the oxidant outlet. One can hypothesize that the shorter the distance of the hole to the exhaust, the lesser the reaction of the transfer hydrogen leak with air inside the cell.

4.5. Comparing oxygen concentration with dP

As shown in Fig. 12, the change in parameters at 20 A for oxygen concentration and dP are somewhat related. The leaky cells had

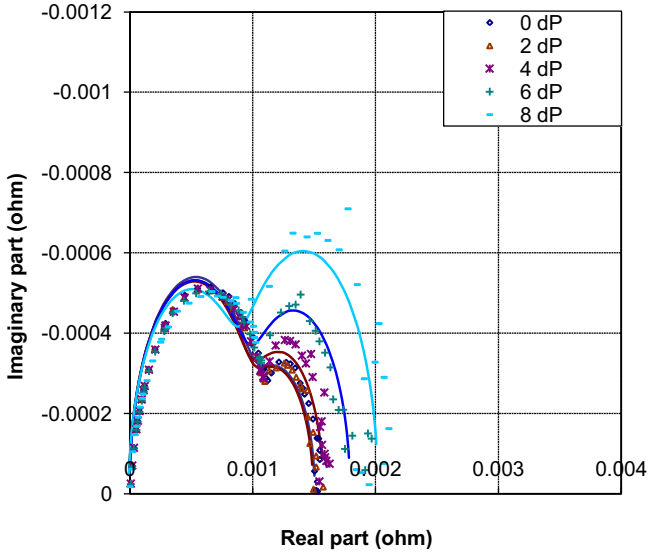

Fig. 10. 50 A impedance of the medium leaky with holes located at the inlet at different dP.

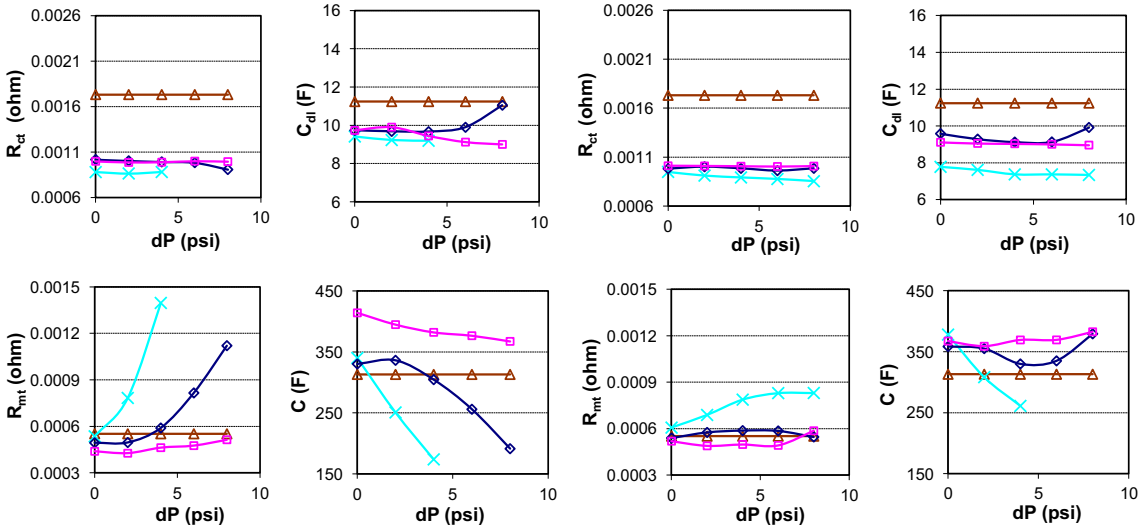

Fig. 11. Effect of differential pressure on the parameters of the 50 A at inlet (left) and outlet (right) ports, (Δ normal cell, □ small leaky cell, ◇ medium leaky cell, ☐ large leaky cell).

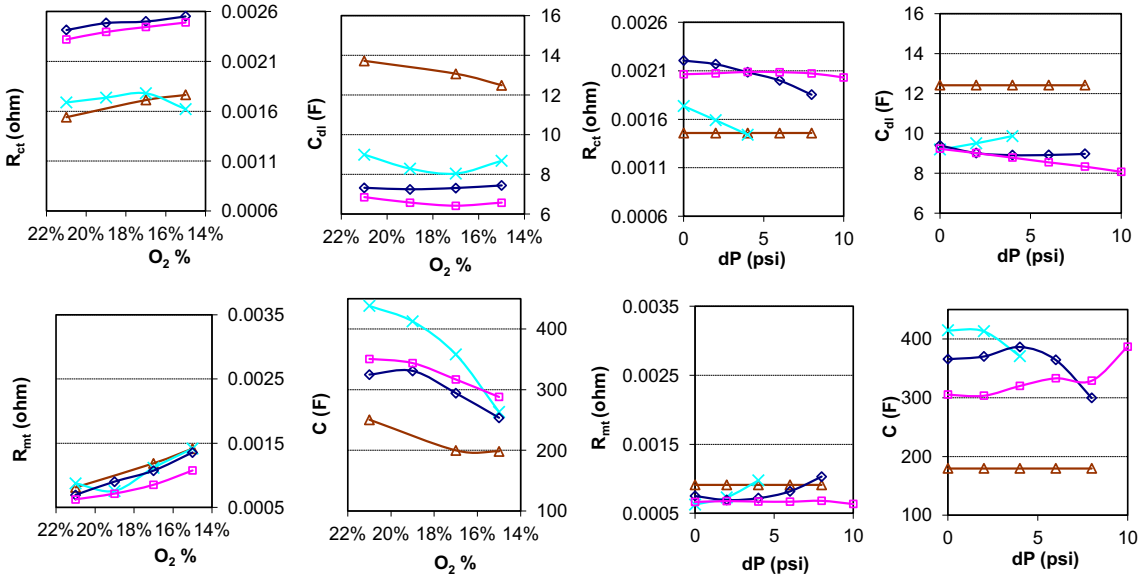

Fig. 12. Effect of oxygen concentration (left) and dP (right) on the parameters of the 20A, (▲normal cell, ■ small leaky cell, ◆ medium leaky cell, ☐ large leaky cell).

lower C_{dl} compared the normal cell, signifying catalyst degradation. The change in R_{mt} with the change in oxygen concentration and dP was minimal. Similarly R_{mt} increased and C decreased due to oxygen mass transport limitations The change in C and R_{mt} with oxygen concentration agreed with the findings by Kawaji et al. [8] and show a significant sensitivity to the oxygen concentration as expected. At lower oxygen concentration, R_{ct} while it decreased with the increasing of leak rates across the MEA due to parasitic current. One can figure out that oxygen concentration and dP have similar behavior in the mass transport region while they are differ in the charge transfer region.

5. Conclusion

EIS was able to detect hydrogen leaks and oxygen concentrations in a single cell very effectively. During air-starvation, the EIS signature was very distinctive especially with full starvation where impedance values were high. With the increase of hydrogen leak rates, the impedance signatures changed mostly in the mass transport region. However, the signatures did not change much when the holes were located at the cathode outlet port of the stack.

This study helped identify the important parameters associated with the existence of leaks in a single cell. Based on these findings, we are convinced that reverse potential faults and the outcomes thereof, can be detected using EIS methods for series of cells. Future study will measure the impedance of a short stack with different numbers of cells and leak rates.

Acknowledgment

The authors would like to thank the Automotive Partnership Canada and Ballard Power Systems for their support of this research. The first author is grateful for a grant from King Abdulaziz University.

The authors are also grateful to Dr. Amir Niroumand, Professor Erik Kjeang, Daniel Zwart and all SFU Co-op students who assisted with this work.

References

[1] H. Tang, Z. Qi, M. Ramani, J.F. Elter, J. Power Sources 158 (2006) 1306–1312.
[2] N. Yousfi-Steiner, Ph. Mocoteguy, D. Candussoc, D. Hissel, J. Power Sources 194 (2009) 130–145.
[3] J. Wu, X.Z. Yuan, H. Wang, M. Blanco, J.J. Martin, J. Zhang, Part I, Int. J. Hydrogen Energy 33 (2008) 1735–1746. Part II, Int. J. Hydrogen Energy 33 (2008) 1747–1757.
[4] C. Brunetto, A. Moschetto, G. Tina, Electr. Power Syst. Res. 79 (2009) 17–26.
[5] J. Kang, D.W. Jung, S. Park, J. Lee, J. Ko, J. Kim, Int. J. Hydrogen Energy 35 (2010) 3727–3735.
[6] X. Yuan, C. Song, H. Wang, J. Zhang, Electrochemical Impedance Spectroscopy in PEM Fuel Cells, Fundamentals and Applications, Springer-Verlag, London, 2010.
[7] M. Ciureanu, R. Roberge, J. Phys. Chem. 105 (2001) 3531–3539.
[8] J. Kawaji, S. Suzuki, Y. Takamori, T. Mizukami, M. Morishima, J. Electrochem. Soc. 158 (2011) 1042–1049.
[9] R. Makharia, M.F. Mathias, D.R. Baker, J. Electrochem. Soc. 152 (2005) 970–977.
[10] U. Cano-Castillo, A. Ortiz, S. Cruz, L.G. Arriaga, G. Orozco, J. Electrochem. Soc. 3 (2006) 931–939.
[11] S.J. Andreasen, J.L. Jespersen, E. Schaltz, S.K. Kær, Fuel Cells 09 (4) (2009) 463–473.
[12] X. Yuan, J.C. Sun, M. Blanco, H. Wang, J. Zhang, D.P. Wilkinson, J. Power Sources 161 (2006) 920–928.
[13] A.M. Dhirde, N.V. Dale, H. Salehfar, M.D. Mann, T. Han, IEEE Trans. Energy Convers. 25 (2010) 3.
[14] J. Lebæk Jespersen, E. Schaltz, S.K. Kær, J. Power Sources 191 (2009) 289–296.
[15] S. Rodat, S. Sailler, F. Druart, P.-X. Thivel, Y. Bultel, P. Ozil, J. Appl. Electrochem. 40 (2010) 911–920.
[16] N. Yousfi-Steiner, Ph. Mocoteguy, D. Candusso, D. Hissel, A. Hernandez, A. Aslanides, J. Power Sources 183 (2008) 260–274.
[17] S. Asghari, A. Mokmeli, M. Samavati, Int. J. Hydrogen Energy 35 (2010) 9283–9290.
[18] M. Boillot, C. Bonnet, N. Jatroudakis, P. Carre, S. Didierjean, F. Lapicque, Fuel Cells 06 (1) (2006) 31–37.
[19] M.R. Ashraf Khorasani, S. Asghari, A. Mokmeli, M.H. Shahsamandi, B.F. Imani, Int. J. Hydrogen Energy 35 (2010) 9269–9275.
[20] G. Tian, S. Wasterlain, D. Candusso, F. Harel, D. Hissel, X. Francois, Int. J. Hydrogen Energy 35 (2010) 2772–2776.